Higher-order sidebands in optomechanically induced transparency

Hao Xiong, Liu-Gang Si, An-Shou Zheng, Xiaoxue Yang, and Ying Wu

Phys. Rev. A **86**, 013815 — Published 11 July 2012

DOI: 10.1103/PhysRevA.86.013815

Higher-order sidebands in optomechanically induced transparency

Hao Xiong,[1,*] Liu-Gang Si,[1,†] An-Shou Zheng,[1,2] Xiaoxue Yang,[1] and Ying Wu[1]

[1]*Wuhan National Laboratory for Optoelectronics and School of Physics, Huazhong University of Science and Technology, Wuhan, 430074, P. R. China*

[2]*College of Mathematics and Physics, China University of Geosciences, Wuhan 430074, P. R. China*

Higher-order sidebands in optomechanically induced transparency is discussed in a generic optomechanical system. We take account nonlinear terms and give an effective method to deal with such problem. It is shown that if a strong control field with frequency ω_1 and a weak probe field with frequency ω_p are incident upon the optomechanical system, then there are output fields with frequencies $\omega_1 \pm 2\Omega$ generation, where $\Omega = \omega_p - \omega_1$. We analyze the amplitude of the output field $\omega_1 + 2\Omega$ varies with the control field, and show that the amplitude of the second-order sideband can be controlled by the strong control field.

PACS numbers: 03.65.Ta, 42.50.Wk

I. INTRODUCTION

Optomechanical system is a rapidly growing field, and many theoretical [1–29] and experimental [30–41] analysis have been done. Figure 1(a) shows a schematic diagram of a generic optomechanical system. The optomechanical system consists of an optical cavity, in which one mirror of the cavity is movable with the angular frequency Ω_m and the mass m. This optomechanical system is driven by a strong control field with frequency ω_1 and a weak probe field with frequency ω_p. This emerging subject leads some remarkable and interesting topics, such as cooling of micromechanical cantilevers to the ground state of motion [1–4], gravitational-wave detectors [5], and optomechanically induced transparency [10, 11, 30, 31] which is an analogue of electromagnetically induced transparency. Electromagnetically induced transparency (EIT), which is original discovered in atomic vapors, leads to many important developments in optical physics [42–46], and has been reported in many different systems [47, 48]. It has been demonstrated recently that a form of induced transparency enabled by the radiation-pressure coupling of an optomechanical system, and such effect is called optomechanically induced transparency (OMIT).

OMIT is a very interesting phenomenon, and can be explained by the Heisenberg-Langevin equations. According to this topic, many fundamental works have been done [6–9]. The Heisenberg-Langevin equations are nonlinear, and it is very difficult to get an analytic solution of these equations. If the probe field is far weaker than the control field, one can use the perturbation method to deal with such problem. Considering that the control field provides a steady-state solution of the system, and we write the intracavity field and the mechanical displacement at the steady-state as $\bar{a}$ and $\bar{x}$. The probe field can be simply considered as a perturbation of the control field. The total solution of the intracavity field and the mechanical displacement under both the control and probe field can be written as $a = \bar{a} + \delta a$ and $x = \bar{x} + \delta x$. Using the linearization of the Heisenberg-Langevin equations, OMIT can be described. In the present work, we take account the nonlinear terms $-iG\delta x\delta a$ and $\frac{\hbar G}{m}\delta a^*\delta a$, where G is the coupling constant which describes the coupling between the cavity field and the movable mirror, and give an effective method to deal with the problem of higher-order sidebands in OMIT. These terms are ignored in most studies [1–30], while we show that these nonlinear terms can lead some interesting phenomena of optomechanical system, such as second and higher-order sidebands [49, 50].

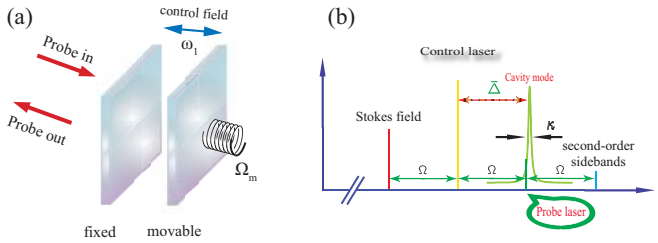

FIG. 1: (Color online) (a) Schematic diagram of a generic optomechanical system. The optomechanical system is driven by a strong control field with frequency ω_1. If the weak probe field with frequency ω_p are incident upon the optomechanical system, then there are some interesting phenomena occur, such as optomechanically induced transparency. (b) Frequency spectrogram of a generic optomechanical system. The frequency of the control field, as shown by the yellow line, is detuned by $\bar{\Delta}$ from the cavity resonance frequency which has a linewidth of κ. We choose that $\bar{\Delta}$ approximately equals to $-\Omega_m$, and $\omega_p - \omega_1$, which recorded as Ω, is over the optical resonance of the cavity. There are higher-order sidebands in such a generic optomechanical system due to the nonlinear terms $-iG\delta x\delta a$ and $\frac{\hbar G}{m}\delta a^*\delta a$.

Figure 1(b) shows the frequency spectrogram of a generic optomechanical system. The frequency of the control field, as shown by the yellow line, is detuned by $\bar{\Delta}$ from the cavity resonance frequency which has a linewidth of κ. The first upper sideband with respect to the pump, viz. control field, is referred to as the anti-Stokes field, while the first lower sideband as the Stokes field. We choose that $\bar{\Delta}$ approximately equals to $-\Omega_m$, and ω_p is offset by the tunable frequency Ω from ω_1. There are higher-order sidebands in such a generic optomechanical system due to the nonlinear terms $-iG\delta x\delta a$ and $\frac{\hbar G}{m}\delta a^*\delta a$. The higher-order sideband processes is that if

*Electronic address: haoxiong1217@gmail.com
†Electronic address: siliugang@gmail.com

the strong control field with frequency ω_1 and the weak probe field with frequency ω_p are incident upon the optomechanical system, then there are output fields with frequencies $\omega_1 \pm n\Omega$ generation, where n is a integer. The output fields with frequencies $\omega_1 \pm 2\Omega$ simply as the second upper and lower sidebands. In the present work, we only focus on the second-order upper sideband. We show that higher-order sidebands can also be tuned by the strong control field.

II. DERIVATION OF HIGHER-ORDER SIDEBANDS IN OPTOMECHANICALLY INDUCED TRANSPARENCY

In this section, we will give a full description of the derivation of higher-order sidebands in optomechanically induced transparency. We begin our discussion by introducing the Hamiltonian formulation of a generic optomechanical system [10, 30]:

$$H = \frac{\hat{p}^2}{2m} + \frac{m\Omega_m^2\hat{x}^2}{2} + i\hbar\sqrt{\eta_c\kappa}\varepsilon_1(\hat{a}^\dagger e^{-i\omega_1 t} - \hat{a}e^{i\omega_1 t}) + i\hbar\sqrt{\eta_c\kappa}(\hat{a}^\dagger\varepsilon_p e^{-i\omega_p t} - \hat{a}\varepsilon_p^* e^{i\omega_p t}) + \hbar\omega_c\hat{a}^\dagger\hat{a} + \hbar G x\hat{a}^\dagger\hat{a}, \quad (1)$$

where $\hat{p}$ and $\hat{x}$ are the momentum and position operators of the movable mirror with effective mass m and angular frequency Ω_m. The term $\hbar\omega_c\hat{a}^\dagger\hat{a}$ is the free Hamiltonian of the cavity field and the term $\hbar G x\hat{a}^\dagger\hat{a}$ denotes the interaction between the cavity field and the movable mirror. The terms $i\hbar\sqrt{\eta_c\kappa}\varepsilon_1(\hat{a}^\dagger e^{-i\omega_1 t} - \hat{a}e^{i\omega_1 t}) + i\hbar\sqrt{\eta_c\kappa}(\hat{a}^\dagger\varepsilon_p e^{-i\omega_p t} - \hat{a}\varepsilon_p^* e^{i\omega_p t})$ describes the driving field, and in the present work it contains a strong control field and a weak probe field. The amplitudes of the pump field and the probe field are normalized to a photon flux at the input of the cavity [30], and defined as $\varepsilon_1 = \sqrt{P_1/\hbar\omega_1}$ and $\varepsilon_p = \sqrt{P_p/\hbar\omega_p}$, where P_1 is the pump power, and P_p is the power of the probe field. κ is the total loss rate which contains an intrinsic loss rate κ_0 and an external loss rate κ_{ex}. The coupling parameter $\eta_c = \kappa_{ex}/(\kappa_0 + \kappa_{ex})$, which can be continuously adjusted, is chosen to be critical coupling 1/2 here, with the best contrast achieved [30].

In a frame rotating at ω_1, the Heisenberg-Langevin equations read [30]:

$$\dot{\hat{a}} = (i\Delta - iGx - \kappa/2)\hat{a} + \sqrt{\eta_c\kappa}\varepsilon_1 + \sqrt{\eta_c\kappa}\varepsilon_p e^{-i\Omega t} + \hat{a}_{in}, \quad (2)$$

$$\dot{\hat{x}} = \hat{p}/m, \quad (3)$$

$$\dot{\hat{p}} = -m\Omega_m^2\hat{x} - \hbar G\hat{a}^\dagger\hat{a} - \Gamma_m\hat{p} + \hat{F}_{th}, \quad (4)$$

where $\Delta = \omega_1 - \omega_c$ and $\Omega = \omega_p - \omega_1$, and the decay rates of the cavity field (κ) and mechanical oscillators (Γ_m) are introduced classically. The quantum noise of the mirror and cavity are described by $\hat{a}_{in}$ and $\hat{F}_{th}$ with $\langle\hat{a}_{in}(t)\hat{a}_{in}^\dagger(t')\rangle = \delta(t-t')$, $\langle\hat{a}_{in}(t)\rangle = 0$, $\langle\hat{F}_{th}(t)\hat{F}_{th}^\dagger(t')\rangle = \Gamma_m\int e^{-i\omega(t-t')}[\coth(\hbar\omega/2k_BT) + 1]d\omega/2\pi\Omega_m$ and $\langle\hat{F}_{th}(t)\rangle = 0$. In this work, we are interested in the mean response of the system to the probe field, so the operators can be reduced to their expectation values, viz. $a(t) \equiv \langle\hat{a}(t)\rangle$, $a^*(t) \equiv \langle\hat{a}^\dagger(t)\rangle$, $x(t) \equiv \langle\hat{x}(t)\rangle$, and $p(t) \equiv \langle\hat{p}(t)\rangle$. In this case we reduce the operator equations to the mean value equations, and drop the quantum and thermal noise terms because $\langle\hat{a}_{in}(t)\rangle = 0$ and $\langle\hat{F}_{th}(t)\rangle = 0$. The Heisenberg-Langevin equations then become:

$$\dot{a} = (i\Delta - iGx - \kappa/2)a + \sqrt{\eta_c\kappa}\varepsilon_1 + \sqrt{\eta_c\kappa}\varepsilon_p e^{-i\Omega t}, \quad (5)$$

$$\dot{x} = p/m, \quad (6)$$

$$\dot{p} = -m\Omega_m^2 x - \hbar G a^\dagger a - \Gamma_m p, \quad (7)$$

For the case that the control field is much stronger than the probe field, we can use the perturbation method to deal with Eqs. (5) - (7). The control field provides a steady-state solution ($\bar{a}$, $\bar{x}$) of the system, while the probe field is treated as the noise, or perturbation of the steady-state. The total solution of the intracavity field and the mechanical displacement under both the control and probe field can be written as $a = \bar{a} + \delta a$ and $x = \bar{x} + \delta x$. The steady-state solution of Eqs. (5) - (7) can be obtained as:

$$\bar{a} = \frac{\sqrt{\eta_c\kappa}\varepsilon_1}{-i\bar{\Delta} + \kappa/2}, \quad \bar{x} = -\frac{\hbar G|\bar{a}|^2}{m\Omega_m^2}, \quad (8)$$

where $\bar{\Delta} = \Delta - G\bar{x}$. Equations (8) give functions mapping the intracavity photon number $|\bar{a}|^2$ to the displacement $\bar{x}$. This system has bistability if the control field is strong enough. Figure 2 shows the displacement $\bar{x}$ varies with the power of the control field by solving Eqs. (8) numerically. We use m=20 ng, $G/2\pi$=-12 GHz/nm, $\Gamma_m/2\pi$=41.0 kHz, $\kappa/2\pi$=15.0 MHz, $\Omega_m/2\pi$=51.8MHz, and Δ=$-\Omega_m$. All of these parameters are chosen from the recent experiment [30]. The wavelengh of the control field is chosen to be 532 nm. It can know that for the case $P_1 < 18$ mW, only one solution exists and the system has no bistability. For the case P_1 is larger than 18 mW while less than 150 mW, there are three solutions exist and the green dashed line indicates the unstable solutions. So the system gives rise to bistability in this case. To obtain an OMIT, the one solution region should be chosen, and we hold $P_1 <$ 18 mW throughout the work.

Now we turn to consider the perturbation made by the probe field. By using $a = \bar{a}+\delta a$ and $x = \bar{x}+\delta x$, Eqs. (5) - (7) become:

$$\frac{d}{dt}\delta a = \Theta\delta a - iG(\bar{a}\delta x + \delta x\delta a) + \sqrt{\eta_c\kappa}\varepsilon_p e^{-i\Omega t},$$
$$\hat{\Psi}\delta x = -\frac{\hbar G}{m}(\bar{a}\delta a^* + \bar{a}^*\delta a - \delta a^*\delta a), \quad (9)$$

where $\Theta = i\Delta - iG\bar{x} - \kappa/2$ and $\hat{\Psi} = \frac{d^2}{dt^2} + \Gamma_m\frac{d}{dt} + \Omega_m^2$. In what follows, we will show that the nonlinear terms $-iG\delta x\delta a$ and $\frac{\hbar G}{m}\delta a^*\delta a$ can lead some interesting effects of optomechanical system.

We solve the problem of inputting a probe field $\varepsilon_p e^{-i\Omega t}$ by using the ansatz:

$$\delta a = \delta a^{(1)} + \delta a^{(2)} + \cdots,$$
$$\delta a^* = \delta a^{*(1)} + \delta a^{*(2)} + \cdots,$$
$$\delta x = \delta x^{(1)} + \delta x^{(2)} + \cdots, \quad (10)$$

where $\delta a^{(1)} = A_1^- e^{-i\Omega t} + A_1^+ e^{i\Omega t}$, $\delta a^{(2)} = A_2^- e^{-2i\Omega t} + A_2^+ e^{2i\Omega t}$, $\delta a^{*(1)} = (A_1^+)^* e^{-i\Omega t} + (A_1^-)^* e^{i\Omega t}$, $\delta a^{*(2)} = (A_2^+)^* e^{-2i\Omega t} + (A_2^-)^* e^{2i\Omega t}$, $\delta x^{(1)} = X_1 e^{-i\Omega t} + X_1^* e^{i\Omega t}$, and $\delta x^{(2)} = X_2 e^{-2i\Omega t} +$

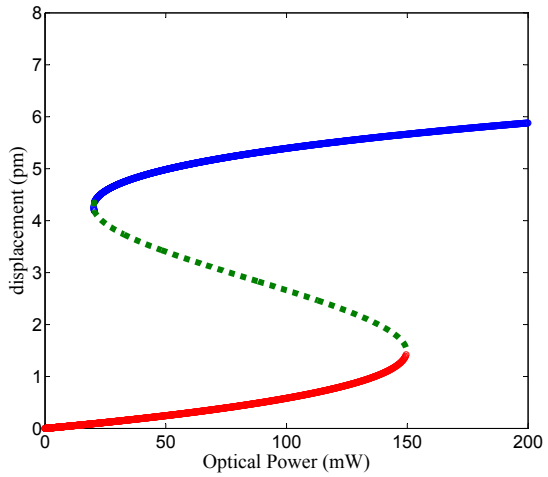

FIG. 2: (Color online) Calculation results of the solutions of Eqs. (8). Here we plot $\bar{x}$ under different P_1. The green dashed line indicates the unstable solutions. We use m=20 ng, $G/2\pi$=-12 GHz/nm, $\Gamma_m/2\pi$=41.0 kHz, $\kappa/2\pi$=15.0 MHz, $\Omega_m/2\pi$=51.8MHz, and Δ=$-\Omega_m$.

$X_2^* e^{2i\Omega t}$. The physical picture of such ansatz is that there are output fields with frequencies $\omega_1 \pm n\Omega$ generation, due to the nonlinear terms $-iG\delta x\delta a$ and $\frac{\hbar G}{m}\delta a^*\delta a$, where n is a integer. If one ignores such nonlinear terms, then the terms of higher-order sidebands in the ansatz can not be self-consistent. In the present work, we only consider the second-order sideband, and higher-order sidebands (for example, 3Ω) are ignored. So we can simplify the ansatz as follows:

$$\begin{aligned}\delta a &= A_1^- e^{-i\Omega t} + A_1^+ e^{i\Omega t} + A_2^- e^{-2i\Omega t} + A_2^+ e^{2i\Omega t},\\ \delta a^* &= (A_1^+)^* e^{-i\Omega t} + (A_1^-)^* e^{i\Omega t} + (A_2^+)^* e^{-2i\Omega t} + (A_2^-)^* e^{2i\Omega t},\\ \delta x &= X_1 e^{-i\Omega t} + X_1^* e^{i\Omega t} + X_2 e^{-2i\Omega t} + X_2^* e^{2i\Omega t}.\end{aligned} \tag{11}$$

In what follows, we will solve Eqs. (9) by using the ansatz (11) and give the amplitude of the second-order sideband. Substituting Eqs. (11) into Eqs. (9) leads six equations:

$$\begin{aligned}(\Theta + i\Omega)A_1^- &= iG(\bar{a}X_1 + X_1^* A_2^- + X_2 A_1^+) - \sqrt{\eta_c\kappa}\varepsilon_p,\\ (\Theta - i\Omega)A_1^+ &= iG(\bar{a}X_1^* + X_1 A_2^+ + X_2^* A_1^-),\\ (\Theta + 2i\Omega)A_2^- &= iG(\bar{a}X_2 + X_1 A_1^-),\\ (\Theta - 2i\Omega)A_2^+ &= iG(\bar{a}X_2^* + X_1^* A_1^+),\\ (\Omega_m^2 - \Omega^2 - i\Gamma_m\Omega)X_1 &= -\frac{\hbar G}{m}\\ &\quad\times\Big(\bar{a}(A_1^+)^* + \bar{a}^* A_1^- - (A_1^-)^* A_2^- - (A_2^+)^* A_1^+\Big),\\ (\Omega_m^2 - 4\Omega^2 - 2i\Gamma_m\Omega)X_2 &=\\ &\quad -\frac{\hbar G}{m}\Big(\bar{a}(A_2^+)^* + \bar{a}^* A_2^- - (A_1^+)^* A_1^-\Big).\end{aligned} \tag{12}$$

We consider that such second-order sideband is a second order processes and whose amplitude is much smaller than the probe field, so we can simplify these six equations into two groups: one group describes the part of linear case

$$\begin{aligned}(\Theta + i\Omega)A_1^- &= iG\bar{a}X_1 - \sqrt{\eta_c\kappa}\varepsilon_p,\\ (\Theta - i\Omega)A_1^+ &= iG\bar{a}X_1^*,\\ (\Omega_m^2 - \Omega^2 - i\Gamma_m\Omega)X_1 &= -\frac{\hbar G}{m}\Big(\bar{a}(A_1^+)^* + \bar{a}^* A_1^-\Big),\end{aligned} \tag{13}$$

and the another describes the part of second-order sideband

$$\begin{aligned}(\Theta + 2i\Omega)A_2^- &= iG(\bar{a}X_2 + X_1 A_1^-),\\ (\Theta - 2i\Omega)A_2^+ &= iG(\bar{a}X_2^* + X_1^* A_1^+),\\ (\Omega_m^2 - 4\Omega^2 - 2i\Gamma_m\Omega)X_2 &= -\frac{\hbar G}{m}\Big(\bar{a}(A_2^+)^* + \bar{a}^* A_2^- - (A_1^+)^* A_1^-\Big).\end{aligned} \tag{14}$$

The equations (13) have been obtained in some previous works [30], and are used to study the effect of optomechanically induced transparency. It can easily solve the equations and obtain A_1^- and X_1 as follows:

$$\begin{aligned}A_1^- &= \frac{1 + if(\Omega)}{\kappa/2 - i(\bar{\Delta} + \Omega) + 2\bar{\Delta}f(\Omega)}\sqrt{\eta_c\kappa}\varepsilon_p,\\ X_1 &= \frac{-\hbar G\bar{a}\chi(\Omega)}{\kappa/2 - i(\bar{\Delta} + \Omega) + 2\bar{\Delta}f(\Omega)}\sqrt{\eta_c\kappa}\varepsilon_p,\end{aligned} \tag{15}$$

where $\chi(\Omega) = 1/m(\Omega_m^2 - \Omega^2 - i\Gamma_m\Omega)$ and $f(\Omega) = \hbar G^2|\bar{a}|^2\chi(\Omega)/[\kappa/2 + i(\bar{\Delta} - \Omega)]$.

The equations (14) describe the second-order sideband of such optomechanical system. We also can solve the equations and obtain A_2^-. It reads

$$A_2^- = \frac{G^2\bar{a}f^{(2)}(\Omega)X_1^2 + GA_1^- X_1\Big(f^{(2)}(\Omega)(i\kappa + 3\Omega - 2\bar{\Delta}) - 1\Big)}{2\bar{\Delta}f^{(2)}(\Omega)(-\bar{\Delta} + \Omega + i\kappa/2) - (\bar{\Delta} + 2\Omega + i\kappa/2)}, \tag{16}$$

with

$$f^{(2)}(\Omega) = \frac{\hbar G^2|\bar{a}|^2\chi(2\Omega)}{(-\bar{\Delta} + \Omega + i\kappa/2)(-\bar{\Delta} + 2\Omega + i\kappa/2)}. \tag{17}$$

Equation (16) is made up of two terms: the first term is a direct second-order sideband, and the other term is an upconverted first-order sideband. The direct second-order sideband, whose amplitude is proportional to $G^2\bar{a}X_1^2$, arise from the two-phonon upconverted process of the control field.

By using the input-output notation, we can obtain the output fields as follows:

$$\begin{aligned}s_{out} &= c_1 e^{-i\omega_1 t} + c_p e^{-i\omega_p t} - \sqrt{\eta_c\kappa}A_2^- e^{-i(2\omega_p - \omega_1)t}\\ &\quad - \sqrt{\eta_c\kappa}A_1^+ e^{-i(2\omega_1 - \omega_p)t} - \sqrt{\eta_c\kappa}A_2^+ e^{-i(3\omega_1 - 2\omega_p)t},\end{aligned} \tag{18}$$

where $c_1 = \varepsilon_1 - \sqrt{\eta_c\kappa}\bar{a}$, $c_p = \varepsilon_p - \sqrt{\eta_c\kappa}A_1^-$. The term of $c_1 e^{-i\omega_1 t}$ and $c_p e^{-i\omega_p t}$ describe the output fields with the frequencies of ω_1 and ω_p respectively. The transmission of the probe field is defined as $t_p = c_p/\varepsilon_p$. Some previous works [30] have used c_p to study OMIT. It can be obtain that

$$t_p = 1 - \frac{1 + if(\Omega)}{\kappa/2 - i(\bar{\Delta} + \Omega) + 2\bar{\Delta}f(\Omega)}\eta_c\kappa. \tag{19}$$

The term of $-\sqrt{\eta_c\kappa}A_1^+e^{-i(2\omega_1-\omega_p)t}$ describes the Stokes process, and has been studied in Ref. [6]. The term of $-\sqrt{\eta_c\kappa}A_2^-e^{-i(2\omega_p-\omega_1)t}$ describes the second-order upper sideband process, in which the output field with the frequency $\omega_1+2\Omega$ can be produced, while the term of $-\sqrt{\eta_c\kappa}A_2^+e^{-i(3\omega_1-2\omega_p)t}$ describes the second-order lower sideband process, in which the output field with the frequency $\omega_1-2\Omega$ can be produced. In what follows, we will give a discussion on the amplitude of the second-order upper sideband. One also can discuss the amplitude of the second-order lower sideband by using the same method.

III. DISCUSSION

Now we turn to discuss the amplitude of the second-order upper sideband varies with ε_1, or equivalent P_1. After such discussion we can find that the second-order sideband can also be tuned by the strong control field.

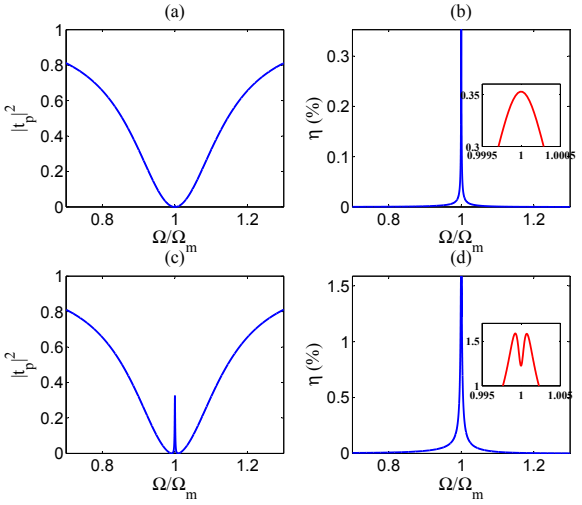

FIG. 3: (Color online) Calculation results of $|t_p|^2$ and η vary with Ω under different ε_1. In Fig. (a) and (b), we use P_1=9.33 μW, while in Fig. (c) and (d), we use P_1=149.3 μW.

The amplitude of the input probe light is ε_p, while the amplitude of the output field with second-order sideband is $|-\sqrt{\eta_c\kappa}A_2^-|$. We define $\eta=|-\sqrt{\eta_c\kappa}A_2^-/\varepsilon_p|$, which is dimensionless, as the efficiency of the second-order sideband process. It should be noted that η, which we choose 20% here for example, is just means that the amplitude of the output second-order sideband is 20% of the amplitude of the input probe light, while not the case of that 20% of the probe light being shifted into the second-order sideband.

Figure 3 shows $|t_p|^2$ and η vary with Ω by using Eq. (16). We use $\varepsilon_p/\varepsilon_1$=0.05, and all of the other parameters are exactly the same as Fig. 2. Figure 3 (a) and (b) shows $|t_p|^2$ and η vary with Ω under the same control field P_1=9.33 μW. In Fig. 3(a) $|t_p|^2$ is very low near Ω/Ω_m=1, which means that the probe field is almost completely absorbed near the resonance condition $\Omega=-\Delta=\Omega_m$. It seems that $|t_p|^2$ reaches its minimum at $\Omega=\Omega_m$, however, if one zooms in sufficiently, there is a local maximum at $\Omega=\Omega_m$. From Fig. 3(b), it can be known that generation of $\omega_1+2\Omega$ is obvious only when the resonance condition $\Omega=\Omega_m$ is reached. Figure 3 (c) and (d) shows $|t_p|^2$ and η vary with Ω under a stronger control field P_1=149.3 μW. Figure 3 (c) shows that there is a transparent window near the resonance condition $\Omega=\Omega_m$, which, however, is not very deep. Figure 3 (d) shows η under the same control field. It can be found that η also become obvious near $\Omega=\Omega_m$. However, on an enlarged scale, a local minimum is

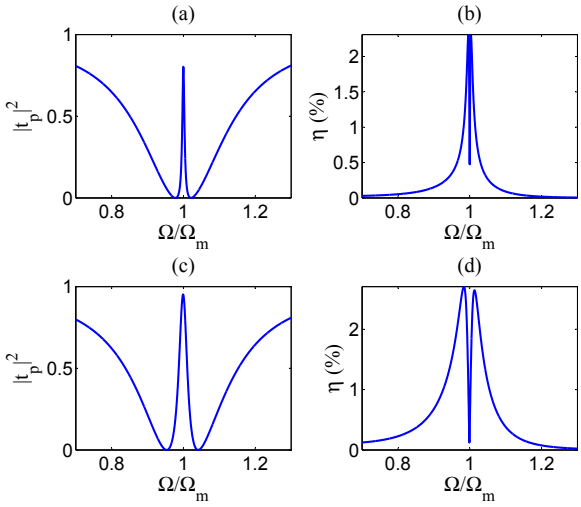

FIG. 4: (Color online) Calculation results of $|t_p|^2$ and η vary with Ω under different ε_1. In Fig. (a) and (b), we use P_1=933.0 μW, while in Fig. (c) and (d), we use P_1=3.7 mW. Other parameters are the same as Fig. 2.

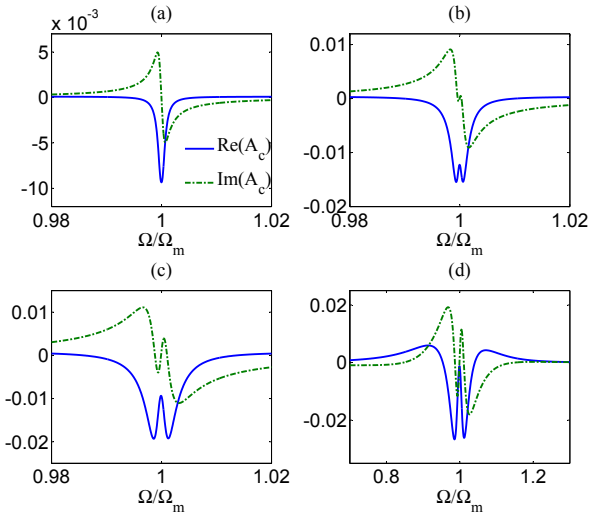

FIG. 5: (Color online) Calculation results of the real and image part of η under different control field ε_1. We use P_1 = (a) 37.3 μW, (b) 149.3 μW, (c) 335.9 μW, (d) 3.7 mW. Other parameters are the same as Fig. 2.

shown.

Now we consider a stronger control field, for example, P_1=933.0 μW. Figure 4 (a) shows $|t_p|^2$ in such a control field. There is a transparent window near the resonance condition $\Omega = \Omega_m$. The transparent window is obvious and much deeper than the case of Fig. 3 (c). Figure 4(b) shows η varies with Ω under the same P_1. Unlike the case shown in Fig. 3(b), in Fig. 4(b) η reaches its local minimum within a frequency window corresponding to about the cavity linewidth at Ω/Ω_m=1. There is a narrow dip near the resonance condition $\Omega = \Omega_m$, in which η become very small. It means that when the OMIT occur, the second-order sideband process is subdued. Such result can also be obtained in Fig. 4(c) and (d). In Fig. 4(c), a control field of P_1=3.7 mW is used. Compared to the case in Fig. 4(a), it can find that the transparent window is wider, and the effect of OMIT is more obvious. Meanwhile, Figure 4(d) shows that the dip is become wider. The value of η at the dip is not exactly zero since Γ_m is nonzero. Taken together Figure 3 and 4 shows that if P_1 is small, and the effect of OMIT does not take place, then the probe field is almost completely absorbed near the resonance condition $\Omega = \Omega_m$, and meanwhile the second-order sideband field achieves the maximum amplitude at $\Omega = \Omega_m$. For the case the effect of OMIT take place, there is a transparent window for the probe field near the resonance condition $\Omega = \Omega_m$, while the second-order sideband field reaches its local minimum within a frequency window corresponding to about the cavity linewidth when Ω/Ω_m=1. It is a suppressive window for the second-order sideband field. As the power of the control field becomes larger, both the transparent window for the probe field and the suppressive window for the second-order sideband field are wider. The real and image part of $A_c \equiv \sqrt{\eta_c\kappa}A_2^-/\varepsilon_p$ under different control fields are shown in Fig. 5. It can find that both the real and image part of $\sqrt{\eta_c\kappa}A_2^-/\varepsilon_p$ have essential changes during the process of turning up the control field. Figure 6 shows the calculation results of $|t_p|^2$ and η vary with the optical power of the control field at the resonance condition $\Omega = \Omega_m$. $|t_p|^2$ increases with the optical power of the control field, while η is not. For the case that the optical power of the control field is weaker than about 0.12 mW, η increases sharply with the optical power of the control field. η reaches its maximum at about P_1 = 0.12 mW. For the case of a larger P_1, η decreases slowly with the optical power of the control field. All of the results, obtained from Fig. 3-6, show that the amplitude of the second-order sideband can be controlled by the strong field ε_1.

Up to now, we have shown that taking account of the nonlinear terms will lead higher-order sidebands in a generic optomechanical system, and the amplitude of the second-order sideband can also be tuned by the strong control field. However, the amplitude of the second-order sideband is very small. Figure 4 shows that the efficiency of the second-order sideband process is only about 2%. It means that the field at the frequency of $\omega_1 + 2\Omega$ is significantly weaker than the probe field. In what follows, we will show that the amplitude of the second-order sideband can be obvious by tuning Δ.

Figure 7 shows the numerical results of $|t_p|^2$ and η vary with Ω by using different Δ. In Fig. 7(a) and (b), we use Δ=$-\Omega_m$,

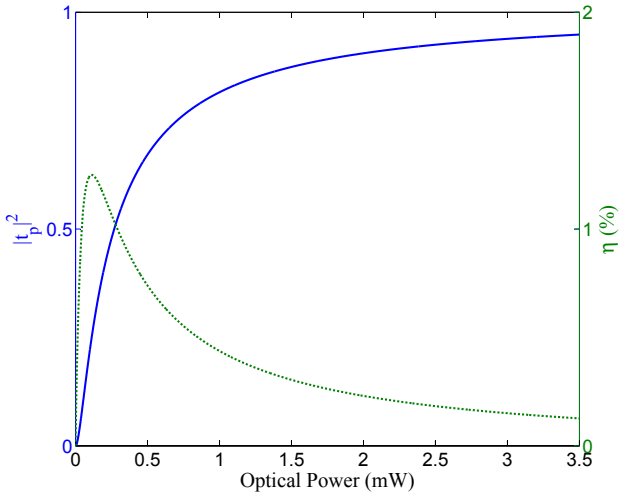

FIG. 6: (Color online) Calculation results of $|t_p|^2$ and η vary with the optical power of the control field at the resonance condition $\Omega = \Omega_m$. We use $\varepsilon_p/\varepsilon_1$=0.05, and all of the other parameters are exact the same as Fig. 2. The blue solid curve represents the calculation results of $|t_p|^2$ while the green dashed curve represents the calculation results of η.

and the results are the same as Fig. 4 (c) and (d). In this case, the efficiency of the second-order sideband process is only about 2%. When we change Δ, the trough of $|t_p|^2$ also changes. In Fig. 7(c) we find that the trough of $|t_p|^2$ is located at $\Omega/\Omega_m \approx$1.4. There is a dip at Ω/Ω_m =1, and it means that the probe field is absorbed greatly in this case. Figure 7(d) shows that there is an obvious second-order sideband at Ω/Ω_m =1, the efficiency of the second-order sideband process is about 15%. Similar results also can be obtained in Fig. 7(e) and (f). It should be noted that Fig. 7 (c) to (f) is not the situation of OMIT. Obviously, there are two absorption peaks in Fig. 7(c) and (e). The first absorption peak is near the resonance condition of the moving mirror $\Omega = \Omega_m$, while the second one is near the resonance condition of the cavity $\Omega = -\bar{\Delta}$. If the resonance condition of the moving mirror is the same as the resonance condition of the cavity, the destructive interference between the probe field photons and the sideband excitations of the control field, which are induced by the mechanical oscillation, causes a tunable transparency window. The detailed process is as follows: The control and probe fields induce a radiation-pressure force oscillating at the frequency Ω, which is the beat frequency between the control and probe fields. If Ω is close to the resonance frequency of the moving mirror Ω_m, the mirror starts to oscillate coherently. As a result, Stokes and anti-Stokes fields will emerge. If the resonance condition of the moving mirror is the same as the resonance condition of the cavity, the anti-Stokes field is resonantly enhanced. So that the probe laser interfere with the anti-Stokes sideband leads a tunable transparency window[30, 33, 41]. If we choose Δ is off-resonance with the anti-Stokes field, here we take Δ=$-1.4\Omega_m$ as an example, then the anti-Stokes field is subdued, and the effect of OMIT is disappeared. However, the

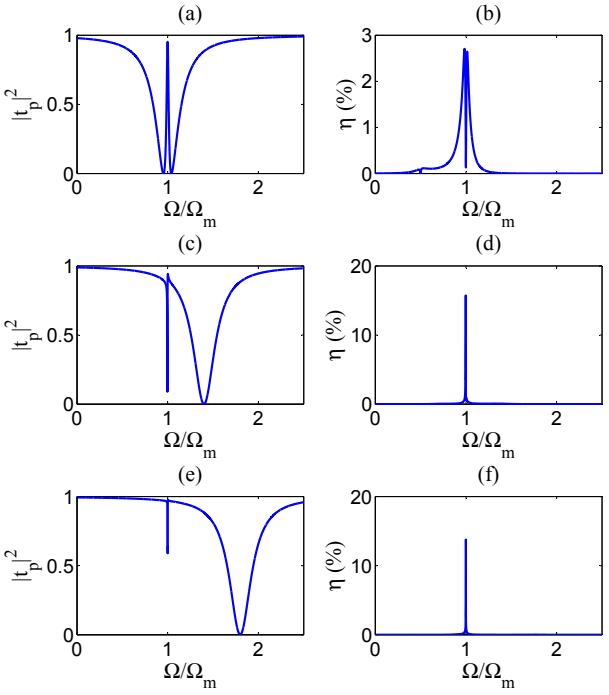

FIG. 7: (Color online) Calculation results of $|t_p|^2$ and η vary with Ω under ε_1=100.0MHz. We use $\Delta=-\Omega_m$ in Fig. (a) and (b), $\Delta=-1.4\Omega_m$ in Fig. (c) and (d), while $\Delta=-1.8\Omega_m$ in Fig. (e) and (f). Other parameters are the same as Fig. 2.

density of states of the cavity field at the second-order sideband is larger than the density of the case $\Delta=-\Omega_m$, so we get a higher η.

The physical interpretation of why the efficiency of the second-order sideband has a local minimum on resonance is that the upconverted first-order sideband process is weak when the OMIT occur, because the destructive interference between the probe field and the anti-Stokes field leads that the cavity field at the frequency Ω is very weak. A mathematical interpretation of why the efficiency of the second-order sideband has a local minimum on resonance can be made by using Eq. (16), which is made up of two terms as having been shown before: the direct second-order sideband term and the upconverted first-order sideband term. If considering $\Omega/\Omega_m \approx 1$, $f^{(2)}(\Omega)$ can be estimated to be the order of $\sim 10^{-12}$. So the first term, which describes the two-phonon upconverted process of the control field, is much smaller than the second term. Then Eq. (16) can be simplified as

$$A_2^- \approx \frac{GA_1^- X_1}{\bar{\Delta} + 2\Omega + i\kappa/2}. \tag{20}$$

It can be obtained that if $\Delta=-\Omega_m$ and when the OMIT occur, then $|A_2^-|$ will reaches the local minimum within a frequency window corresponding to about the cavity linewidth when Ω/Ω_m=1 because both the $|A_1^-|$ and X_1 reach the local minimum in this case. A possible interpretation of the obvious second-order sideband for the case $\Delta \approx$ -1.5 Ω_m is that the density of states of the cavity field at the first- and second-order sidebands is equal when $\Delta \approx$ -1.5 Ω_m. Therefore two-step scattering into the second-order sideband is rendered more probable than it would otherwise be. This result also can be obtained by using the simplified expression of Eq. (16). When we tuning Δ, the effect of OMIT will disappear, and both $|A_1^-|$ and X_1 become larger. More importantly, $\bar{\Delta}+2\Omega$ in the denominator of Eq. (20) is smaller, so it leads an obvious second-order sideband.

IV. CONCLUSION

The propagation of electromagnetic fields in various system is a wide range of issues [41–57]. Optomechanical system is a promising approach to manipulate the propagation of light [41, 49, 50]. In this work, we show that an generic optomechanical system driven by a pump field with frequency ω_1 and a weak probe field with frequency ω_p can lead to generation of second-order sideband signals $\omega_1 \pm 2\Omega$ by taking account nonlinear terms. We give an effective method to calculate the amplitude of such fields. We find that the second-order sidebands can also be tuned by the strong control field. There are some connections between OMIT and the second-order sideband process. When the OMIT occur, the second-order sideband process is subdued. We also show that the amplitude of the second-order sideband can be controlled by the detuning Δ.

Acknowledgments

The work was supported in part by the National Science Foundation (NSF) of China (Grant Nos. 10975054, 91021011, and 11005057), the National Fundamental Research Program of China (Grant No. 2012CB922103), the Research Fund for the Doctoral Program of Higher Education of China (Grant No. 200804870051), and the Fundamental Research Funds for the Central Universities', HUST (Grant No. 2012QN115). H. X. is also supported in part by the Program for Excellent Doctoral Student granted by Ministry of Education China, and the Doctorate Innovation Foundation of the Huazhong University of Science and Technology. We also acknowledge the anonymous referees for their insightful comments.

[1] T. W. Hansch and A. L. Schawlow, Opt. Commun. **13**, 68 (1975).

[2] D. J. Wineland, R. E. Drullinger, and F. L. Walls, Phys. Rev. Lett. **40**, 1639 (1978).

[3] S. Chu, L. Hollberg, J. E. Bjorkholm, A. Cable, and A. Ashkin, Phys. Rev. Lett. **55**, 48 (1985).
[4] R. Rivière, et al., Phys. Rev. A **83**, 063835 (2011).
[5] C. M. Caves, Phys. Rev. Lett. **45**, 75 (1980).
[6] S. Huang and G. S. Agarwal, Phys. Rev. A **81**, 033830 (2010).
[7] T. J. Kippenberg, H. Rokhsari, T. Carmon, A. Scherer, and K. J. Vahala, Phys. Rev. Lett. **95**, 033901 (2005).
[8] V. B. Braginsky, S. E. Strigin, and S. P. Vyatchanin, Phys. Lett. A **287**, 331 (2001).
[9] V. B. Braginsky, S. E. Strigin, and S. P. Vyatchanin, Phys. Lett. A **305**, 111 (2002).
[10] G. S. Agarwal and S. Huang, Phys. Rev. A **81**, 041803 (2010).
[11] S. Huang and G. S. Agarwal, Phys. Rev. A **83**, 043826 (2011).
[12] C. Joshi, J. Larson, M. Jonson, E. Andersson, and P. öhberg, Phys. Rev. A **85**, 033805 (2012).
[13] J.-Q. Liao, H. K. Cheung, and C. K. Law, Phys. Rev. A **85**, 025803 (2012).
[14] F.-Y. Hong, Y. Xiang, W. H. Tang, Z.-Y. Zhu, L. Jiang, and L. Wu, Phys. Rev. A **85**, 012309 (2012).
[15] T. Botter, D. W. C. Brooks, N. Brahms, S. Schreppler, and D. M. Stamper-Kurn, Phys. Rev. A **85**, 013812 (2012).
[16] S. Barzanjeh, M. H. Naderi, and M. Soltanolkotabi, Phys. Rev. A **84**, 063850 (2011).
[17] M. Tomes, F. Marquardt, G. Bahl, and T. Carmon, Phys. Rev. A **84**, 063806 (2011).
[18] S. G. Hofer, W. Wieczorek, M. Aspelmeyer, and K. Hammerer, Phys. Rev. A **84**, 052327 (2011).
[19] J.-Q. Liao, and C. K. Law, Phys. Rev. A **84**, 053838 (2011).
[20] A. Xuereb, R. Schnabel, and K. Hammerer, Phys. Rev. Lett. **107**, 213604 (2011).
[21] B. Chen, C. Jiang, J.-J. Li, and K.-D. Zhu, Phys. Rev. A **84**, 055802 (2011).
[22] S. Zaitsev, A. K. Pandey, O. Shtempluck, and E. Buks, Phys. Rev. E **84**, 046605 (2011).
[23] M. H. Schleier-Smith, I. D. Leroux, H. Zhang, M. A. V. Camp, and V. Vuletić, Phys. Rev. Lett. **107**, 143005 (2011).
[24] S. K. Steinke and P. Meystre, Phys. Rev. A **84**, 023834 (2011).
[25] Q. Sun, X.-H. Hu, W. M. Liu, X. C. Xie, and A.-C. Ji, Phys. Rev. A **84**, 023822 (2011).
[26] H. K. Cheung and C. K. Law, Phys. Rev. A **84**, 023812 (2011).
[27] T. G. McRae, K. H. Lee, G. I. Harris, J. Knittel, and W. P. Bowen, Phys. Rev. A **82**, 023825 (2010).
[28] G. A. T. Pender, P. F. Barker, F. Marquardt, J. Millen, and T. S. Monteiro, Phys. Rev. A **85**, 021802 (2012).
[29] J. Hofer, A. Schliesser, and T. J. Kippenberg, Phys. Rev. A **82**, 031804 (2010).
[30] S. Weis, et al., Science **330**, 1520 (2010).
[31] A. H. Safavi-Naeini, et al., Nature **472**, 69 (2011).
[32] T. P. Purdy, D.W. C. Brooks, T. Botter, N. Brahms, Z.-Y. Ma, and D. M. Stamper-Kurn, Phys. Rev. Lett. **105**, 133602 (2010).
[33] A. Schliesser and T. J. Kippenberg, Physics **4**, 97 (2011).
[34] A. Schliesser, O. Arcizet, R. Rivière, G. Anetsberger, and T. J. Kippenberg, Nature Physics **5**, 509 (2009).
[35] G. Anetsberger, O. Arcizet, Q. P. Unterreithmeier, R. Rivière, A. Schliesser, E. M. Weig, J. P. Kotthaus, and T. J. Kippenberg, Nature Physics **5**, 909 (2009).
[36] G. Anetsberger, R. Rivière, A. Schliesser, O. Arcizet, and T. J. Kippenberg, Nature Photonics **2**, 627 (2008).
[37] Y.-S. Park and H. Wang, Nature Physics **5**, 489 (2009).
[38] I. Favero and K. Karrai, Nature Photonics **3**, 201 (2009).
[39] E. Verhagen, S. Deléglise, S. Weis, A. Schliesser, and T. J. Kippenberg, Nature **482**, 63 (2012).
[40] T. J. Kippenberg and K. J. Vahala, Science **321**, 1172 (2008).
[41] A. Schliesser and T. J. Kippenberg, Adv. At. Mol. Opt. Phys. **58**, 207 (2010).
[42] Y. Wu and X. Yang, Phys. Rev. A **76**, 013832 (2007).
[43] W.-X. Yang, A.-X. Chen, R.-K. Lee, and Y. Wu, Phys. Rev. A **84**, 013835 (2011).
[44] X.-T. Xie and M. A. Macovei, Phys. Rev. Lett. **104**, 073902 (2010).
[45] Y. Wu and X. Yang, Phys. Rev. A **68**, 013608 (2003).
[46] W.-X. Yang, J.-M. Hou, Y. Lin, and R.-K. Lee, Phys. Rev. A **79**, 033825 (2009).
[47] Y. Wu and X. Yang, Phys. Rev. B **76**, 054425 (2007).
[48] Y. Wu and X. Yang, Phys. Rev. A **71**, 053806 (2005).
[49] F. Marquardt, J. G. E. Harris, and S. M. Girvin, Phys. Rev. Lett. **96**, 103901 (2006).
[50] A. Schliesser, R. Rivière, G. Anetsberger, O. Arcizet, and T. J. Kippenberg, Nature Physics **4**, 415 (2008).
[51] H. Xiong, L.-G. Si, P. Huang, and X. Yang, Phys. Rev. E **82**, 057602 (2010).
[52] H. Xiong, L.-G. Si, J. F. Guo, X.-Y. Lü, and X. Yang, Phys. Rev. A **83**, 063845 (2011).
[53] H. Xiong, L.-G. Si, C. Ding, X. Yang and Y. Wu, Phys. Rev. A **84**, 043841 (2011).
[54] H. Xiong, L.-G. Si, C. Ding, X.-Y. Lü, X. Yang and Y. Wu, Phys. Rev. E **85**, 016602 (2012).
[55] H. Xiong, L.-G. Si, C. Ding, X. Yang and Y. Wu, Phys. Rev. E **85**, 016606 (2012).
[56] V. Y. Fedorov and T. Nakajima, Phys. Rev. Lett. **107**, 143903 (2011).
[57] N. Papasimakis, V. A. Fedotov, N. I. Zheludev, and S. L. Prosvirnin, Phys. Rev. Lett. **101**, 253903 (2008).